Available online at www.sciencedirect.com
ScienceDirect
Polymer 48 (2007) 4184–4195
polymer
www.elsevier.com/locate/polymer

Compressive properties of extruded polytetrafluoroethylene

Jennifer L. Jordan [a,*], Clive R. Siviour [b], Jason R. Foley [c], Eric N. Brown [d]

[a] Energetic Materials Branch, Munitions Directorate, Air Force Research Laboratory, Eglin AFB, FL 32542, United States
[b] Department of Engineering Science, University of Oxford, Oxford OX1 3PJ, UK
[c] Fuzes Branch, Munitions Directorate, Air Force Research Laboratory, Eglin AFB, FL 32542, United States
[d] Materials Science and Technology Division, Los Alamos National Lab, Los Alamos, NM 87545, United States

Received 5 April 2007; received in revised form 8 May 2007; accepted 9 May 2007
Available online 21 May 2007

Abstract

Polymers are becoming increasingly used in aerospace structural applications, where they experience complex, non-static loads. Correspondingly, the mechanical properties at high strain rates are of increasing importance in these applications. This paper presents an investigation of the properties of Dupont 9B polytetrafluoroethylene (PTFE) across strain rates from 10^{-3} to 10^{5} s^{-1}. The samples were tested using an Instron mechanical testing machine for static loading, traditional split Hopkinson pressure bars (SHPBs) for high strain rates, and a miniaturized SHPB for ultra-high strain rates. Additionally, the material was tested using dynamic mechanical analysis to determine the effects of time–temperature superposition on the strain rate behavior of the samples. The results of the experiments are analyzed using the Zerilli–Armstrong model for polymers, which shows good agreement with other PTFE studies.

Keywords: Semi-crystalline polymer; High strain rate mechanical properties; Polytetrafluoroethylene

1. Introduction

Polytetrafluoroethylene (PTFE), or Teflon[1], is used in small high-performance parts due to its low coefficient of friction and resistance to wear and chemical corrosion. Although some studies on the compressive properties of PTFE across a range of strain rates and temperatures have been presented in the literature [1–3], until recently importance was not placed on the processing history of the material prior to testing [4–11]. However, the processing route used to prepare the PTFE can greatly affect the crystallinity of the material, which is known to influence the strength and deformation behavior [4,5].

Polytetrafluoroethylene is a complicated semi-crystalline material that undergoes crystalline phase changes at 19 °C from phase II to phase IV and at 30 °C from phase IV to phase I, at ambient pressure [7]. While phases II and IV are rigorously crystalline, phase I is sometimes described as mesophase [12]. In addition, the amorphous PTFE undergoes three relaxations, γ and α, which are similar to glass transitions and β, which encompasses the crystalline phase transitions between phases II, IV, and I [4,13]. PTFE can be thought of as a two-phase structure, similar to a particulate composite, with a ''rigid'' crystalline phase in a matrix of a ''softer'' amorphous phase. Similar to particulate composites, increasing the fraction of crystalline material will increase the strength of the sample. The crystalline phase has been shown to have a strong effect on whether fracture of PTFE is brittle (phase II) or ductile (phases I and IV) [7]. Additionally, the elastic modulus and fracture stress of PTFE has been shown to have a strong pressure dependence [14]. In particular, the pressure dependence of the elastic modulus has been shown to be bilinear resulting from the shift of a low temperature relaxation with applied hydrostatic pressure [14].

The high rate, large-strain mechanical properties of polymers are of great scientific and industrial importance. The first study of the stress–strain behavior of polymers over a wide range of strain rates is usually regarded as being that of Chou et al. [15], who examined the behavior of polymethyl

* Corresponding author. Tel.: +1 850 882 8992; fax: +1 850 882 3540.
E-mail address: jennifer.jordan@eglin.af.mil (J.L. Jordan).
[1] Teflon is a registered trademark of Dupont.

0032-3861/$ - see front matter © 2007 Elsevier Ltd. All rights reserved.
doi:10.1016/j.polymer.2007.05.038

methacrylate (PMMA), cellulose acetate butyrate, polypropylene and nylon 66, in compression, using a 'medium strain-rate machine' and a split Hopkinson pressure bar (SHPB) [15]. In particular, he plotted the mechanical strength of these materials as a function of strain rate. Whilst it was expected that the stress supported at a given strain would be a linear function of $\log(\dot{\varepsilon})$, where $\dot{\varepsilon}$ is the strain rate, it was in fact found that at high rates this stress increased more quickly. An increase in the strain rate dependence of yield stress was also observed by Briscoe and Hutchings [16] and Kukureka and Hutchings [17] for high density polyethylene (HDPE). However, doubt was cast on the validity of the measurements by Briscoe and Nosker, who considered carefully the effects of friction and specimen response in the Hopkinson bar [18,19], and Brown et al. [20], who investigated several forms of polyethylene (PE). They concluded that in fact the yield strength of HDPE is linear in $\log(\dot{\varepsilon})$.

Walley and Field [3] examined the behavior of a large number of polymers, at room temperature, over strain rates ranging from 10^{-2} to $10^{4}\ \mathrm{s}^{-1}$, taking great care to use suitable lubrication and specimen sizes to reduce friction and inertia. Again, they plotted the yield stress as a function of $\log(\dot{\varepsilon})$, and found that the different materials fell into three different groups:

- A linear relationship, with no change at higher strain rates.
- A bilinear behavior with a sharp increase in gradient at a strain rate of $\sim 10^{3}\ \mathrm{s}^{-1}$.
- A decrease in maximum stress at a strain rate of $\sim 10^{3}\ \mathrm{s}^{-1}$, possibly followed by an increase.

In addition to strain rate, temperature has an important effect on the mechanical properties of polymers. Bauwens–Crowet conducted a series of compression experiments on PMMA at rates between 10^{-4} and $1\ \mathrm{s}^{-1}$ [21]. Each of these rate sweeps was repeated every 20 °C between −20 and 100 °C. The dependence of yield stress on strain rate and temperature was reported, and using a time–temperature superposition they extended the range of the experiments to $10^{6}\ \mathrm{s}^{-1}$ at 100 °C. In addition, the material was tested at a strain rate of $4 \times 10^{3}\ \mathrm{s}^{-1}$ over a range of temperatures. Both sets of data showed a bilinear relationship, with increased strength at high strain rates and at low temperatures. In earlier papers, Bauwens and colleagues had investigated PC in compression over a range of temperatures, and found a similar relationship [22,23]. This behavior was attributed to the different molecular relaxations in the material. At high temperatures or low strain rates only the α relaxation (glass transition) plays a role in the polymer behavior, whilst at low temperatures and high strain rates, the effect of the β relaxation is added to that of the α. The authors developed a model to explain the behavior, and this was also used by Rietsch and Bouette [24]. More recently, Siviour et al. [25,26] performed experiments on polycarbonate (PC) and polyvinylidene fluoride (PVDF). Using temperature–strain rate equivalence, they identified how the different molecular transitions affected the strain rate dependence of material strength. An excellent paper by Mulliken and Boyce [27] further showed how shifting data from DMA curves can be used to develop the physically based understanding behind a predictive model for high strain rate behavior of polymers.

Although several models for PTFE have been applied in the literature [28–30], the Zerilli–Armstrong model was chosen for this work due to familiarity with the model. The Zerilli–Armstrong model for polymers [31–36] is based on thermally activated flow under applied shear stress through movement of ''flow units'', which overcome local obstacles (i.e., potential barriers) to displacement. The model addresses the temperature, pressure and strain rate dependence of a 3-D isotropic polymer; neglects the small plastic component of strain in hydrostatic compression, brittleness and fracture associated with low temperature or high strain rate; and includes creep and long term relaxation effects. The viscoelastic component of the model is represented by Maxwell–Weichert linear elements with a non-linear thermal activation dashpot providing a viscoplastic contribution. A detailed presentation of the equations describing this model is presented by Zerilli and Armstrong [36]. For the uniaxial stress (σ) case, assuming an incompressible material, the three-dimensional equations reduce to

$$\dot{\sigma}_{11}^{(k)} + \frac{\sigma_{11}^{(k)}}{\tau_k} = 3G_k\left(\dot{\varepsilon}_{11} - \dot{\varepsilon}_{11}^{(\mathrm{p})}\right), \quad k = 1, 2, \ldots \tag{1}$$

and

$$\sigma_{11} = \sigma_{\mathrm{p}}\left(\dot{\varepsilon}^{(\mathrm{p})}, \varepsilon^{(\mathrm{p})}\right)\frac{\dot{\varepsilon}_{11}^{(\mathrm{p})}}{\left|\dot{\varepsilon}_{11}^{(\mathrm{p})}\right|}, \tag{2}$$

where the sub/superscript k represents the Maxwell–Weichert elements, the sub/superscript p indicates the plastic component of the stress and strain, ε and $\dot{\varepsilon}$ are the strain and strain rate, respectively, K is the volume and temperature dependent bulk modulus, and G_k and τ_k are the modulus and relaxation times of the Maxwell–Weichert elements. The plastic stress is defined by Eqs. (19)–(23) of Zerilli and Armstrong [36].

This paper presents results from recent experiments investigating the quasi-static and high strain rate compressive properties of extruded PTFE rod. The effect of annealing the extruded rod to reduce residual stresses is also investigated. The results are compared to the Zerilli–Armstrong model for polymers.

2. Experimental procedure

2.1. Sample preparation

A 3/4'' diameter rod of ram-extruded Dupont 9B Teflon [37] (Fluoro-plastics, Philadelphia, PA) was machined to make cylindrical compression samples parallel to the extruding direction. The samples were tested in the as-received state as well as after annealing to remove residual stresses from the extrusion process. The annealing regime recommended by the manufacturer is as follows: 28 °C/h to 260 °C, hold 1 h; 14 °C/h to 204 °C, hold 1/2 h; 28 °C/h to room temperature.

2.2. Experimental set-up

The as-received and annealed samples were characterized by differential scanning calorimetry (DSC), thermomechanical analysis (TMA), and dynamic mechanical analysis (DMA) to determine the effects of annealing on the rod. DSC scans were conducted from room temperature to 400 °C at 10 °C/min using a Thermal Analysis Instruments (TAI) model 2920. Thermomechanical analysis, using a TAI model 2940, was run at 5 °C/min on as-received and annealed samples in both the axial (i.e., parallel to the extrusion axis) and radial (perpendicular to the extrusion axis) directions. DMA analysis was performed in a single cantilever configuration at 1, 10, and 100 Hz over temperatures from −125 to 200 °C.

In order to determine the degree of crystallinity in the sample, DSC and density measurements were conducted, as described by Rae and Dattelbaum [4]. By employing the same analysis and material constants it is possible to make direct comparisons between the PTFE 9B reported in the current work and the previously reported work on PTFE 7C [4–11]. The DSC scans were performed using a TAI 2920 Modulated Differential Scanning Calorimeter on ∼10 mg samples with 10 °C/s heating rate. Density measurements were conducted using helium gas pycnometry (Micromeritics Accupyc 1330). For an extensive review of the methods for determining crystallinity in PTFE see Lehnert et al. [38]. More recent work using modulated-DSC have sought to obtain additional insight in the structure of PTFE by separation of the reversible and non-reversible heat flow [39,40]; however, this is beyond the scope of the current work.

The samples were tested across a range of strain rates from 10^{-2} to 10^{4}, at room temperature. An Instron model 1332 was used for quasi-static loading, in which the samples were nominally 8 mm diameter by 3.5 mm thick. It is generally accepted that quasi-static compression samples should have a length to diameter ratio of 2:1. However, in these experiments, samples with dimensions identical to those used for the split Hopkinson pressure bar were tested. The strain in the sample was determined from crosshead displacement, and the stress was determined from the load cell output. All data was acquired using Instron's Merlin software.

Compression experiments at intermediate strain rates (10^{3}–10^{4}) were conducted using two split Hopkinson pressure bars (SHPB) [41,42], a schematic diagram of which can be seen in Fig. 1. The majority of the experiments were conducted using the SHPB system located at AFRL/MNME, Eglin AFB, FL, which is comprised of 1524 mm long, 19 mm diameter incident and transmitted bars of 440-HT stainless steel or 6061-T6 aluminum. The striker is 305 mm long and made of the same material as the other bars. The remainder were performed using the SHPB system at the Cavendish Laboratory, University of Cambridge, which consists of 500 mm long, 12.7 mm diameter incident and transmitted bars with a 200 mm striker bar of grade 300 maraging steel. The samples, which were nominally 8 mm diameter by 3.5 mm thick or 5 mm diameter by 2.5 mm thick, depending on strain rate, are positioned between the incident and transmitted bars. The bar faces were lightly lubricated with paraffin wax to reduce friction. The properties of the stainless steel, aluminum, and maraging steel bars are given in Table 1. The Cavendish system was used, in addition to the Eglin system, in order to utilize the in situ laser diameter measurement system, which is discussed later.

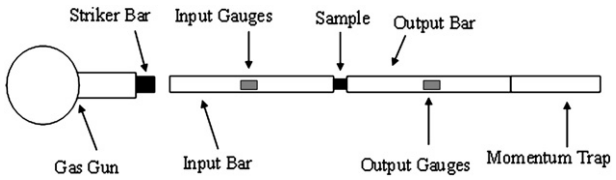

Fig. 1. Schematic of split Hopkinson pressure bar (SHPB) experimental set-up.

Experiments at ultra-high strain rates ($10^{5}\ s^{-1}$) were conducted using a miniaturized split Hopkinson pressure bar (MSHPB), which is, in principle, identical to the full sized SHPB. However, the bars are 300 mm long and 3–3.2 mm in diameter. Samples tested in this apparatus are nominally 1.5 mm diameter by 0.6 mm long. Miniaturized direct impact bar systems have been widely studied [43–45] and Jia and Ramesh [46] recently published a comprehensive analysis of a similar miniature bar system. A major advantage of the split bar system, over direct impact, is that mechanical equilibrium in the specimen may be confirmed by comparing one- and two-wave analyses, as described by Gray [41]. The goal is to have the two-wave stress oscillate around the one-wave stress (see Ref. [41], Fig. 6). This shows that stress state at the two ends of the sample are temporally nominally the same. The concern would be that the two-wave stress would not oscillate around the one-wave stress, which would suggest a stress gradient throughout the material thus making measurement of the material response impossible. In this case, the oscillations are expected. All data in the paper is from the one-wave analysis, which is the traditional presentation of split Hopkinson pressure bar data. The MSHPB, at Eglin AFB, provides the opportunity to test materials up to strain rates of $10^{5}\ s^{-1}$, with tungsten carbide (WC) and titanium alloy (Ti–6Al–4V) bar materials available. The properties of these bar materials are also listed in Table 1.

For all bar systems, the properties of the sample are determined by measuring the incident, reflected, and transmitted

Table 1
Selected properties of the bar materials used in the SHPB and MSHPB

Material	Density ρ (kg/m^3)	Wave speed (acoustic) c (km/s)	Impedance (acoustic) $Z=\rho c$ ($\times 10^7$ kg m^{-2} s^{-1})	Yield stress σ_Y (MPa)
440-HT stainless steel	6157	5.542	3.41	1970
6061-T6 Al	2716	5.039	1.36	290
British maraging steel	8082	4.835	3.90	758
WC	14527	6.316	9.18	2600
Ti6Al4V	2709	5.039	1.37	1000

Density, acoustic wave speed, and impedance are measured from the bar materials. Yield stresses are literature values.

strain signals, ε_I, ε_R, and ε_T, respectively, using Kulite AFP-500-90 semiconductor strain gages. These gages are smaller (1 mm long) than traditional foil gages and have a much higher gage factor (140). The gages form part of a potential divider circuit with constant voltage excitation, which transforms the resistance change of the gages to a voltage change and compensates for temperature changes. The strain gages are dynamically calibrated in situ by performing a number of impacts with carefully measured striker bar velocities. From the measured impact velocity and mass of the striker, the force amplitude of the stress pulse introduced, F, can be determined and compared to the voltage output, V, from the strain gages to give a calibration in the form:

$$F = KV(1 + bV), \tag{3}$$

where K and b are calibration factors.

The full derivation of the data reduction used to calculate the strain rate and stress in the specimen, as functions of time, can be found in Refs. [41,42]. In order to make representative measurements of material properties, it is necessary that the specimen achieves mechanical equilibrium during the experiment, and this is sometimes assumed as it makes the strain rate calculation more straightforward [41]. The software used in the experiments presented in this paper performs the one- and two-wave analyses automatically for every specimen, so stress state equilibrium is verified in every experiment. However, the calculation of strain rate does not assume mechanical equilibrium, rather it uses all three of the incident, reflected and transmitted force pulses to calculate specimen strain rate through the following equation:

$$\dot{\varepsilon}(t) = \left[\frac{C_b}{l_S}\right](\varepsilon_I(t) - \varepsilon_R(t) - \varepsilon_T(t)), \tag{4}$$

where ε_I, ε_R, and ε_T are the incident, reflected and transmitted strain pulses time shifted to the front and rear faces of the specimen, respectively, C_b is the sound speed in the bar material, and l_S is the length of the sample. This specimen strain rate is then integrated to give the strain,

$$\varepsilon(t) = \int_0^t \dot{\varepsilon}(t)\mathrm{d}t, \tag{5}$$

and the transmitted strain pulse is used to calculate the reported one-wave specimen stress,

$$\sigma(t) = \left[\frac{E_b A_b}{A_S}\right]\varepsilon_T(t), \tag{6}$$

where E_b, and A_b are the elastic modulus and cross-sectional area of the bar material, respectively, and A_S is the cross-sectional area of the sample. The two-wave specimen stress is calculated using Eq. (4) with ε_T replaced by $\varepsilon_I + \varepsilon_R$. If true stress is required, A_S is typically updated using the strain calculation, assuming that volume is conserved during deformation.

In order to confirm volume conservation, the diameter of the expanding PTFE specimens was measured in situ on the Cambridge SHPB system using laser diameter measurement [26,47]. The radial expansion measurements can be used to test the constant volume assumption of the SHPB equations. The Poisson's ratio, ν, during the experiment can be calculated by

$$\nu = \frac{\varepsilon_r}{\varepsilon_a}, \tag{7}$$

where ε_r and ε_a are the radial and axial strains, respectively. This is a pragmatic engineering extension of the Poisson's ratio, which is only defined for small elastic strains.

3. Results and discussion

3.1. Thermomechanical analysis and crystallinity

Thermomechanical analysis and differential scanning calorimetry before and after annealing and dynamic mechanical analysis after annealing were conducted on the polytetrafluoroethylene samples, shown in Figs. 2 and 3. PTFE is a complicated material with several phase changes [13]. At atmospheric pressure, PTFE undergoes two crystal–crystal phase transitions from a triclinic crystal structure to a hexagonal structure at 19 °C and from the hexagonal structure to a pseudohexagonal structure at 30 °C. The phase change at 19 °C is evident in the axial TMA scan, particularly in the as-received sample. Crystalline melting is evident from the large endotherm in the DSC scans occurring at 332.8 °C in the as-received material and 330.2 °C in the annealed material compared to 327 °C reported for PTFE [13]. The three

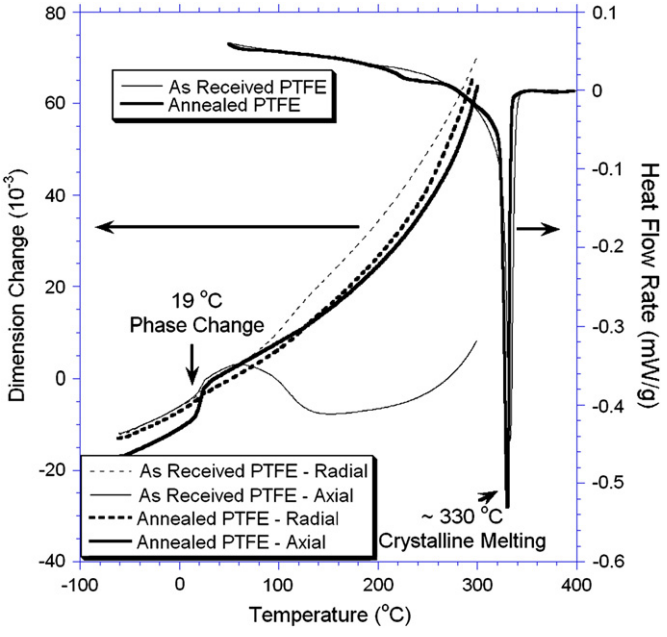

Fig. 2. Thermomechanical analysis (TMA) and differential scanning calorimetry (DSC) showing dimensional change and heat flow, respectively, in PTFE across a range of temperatures.

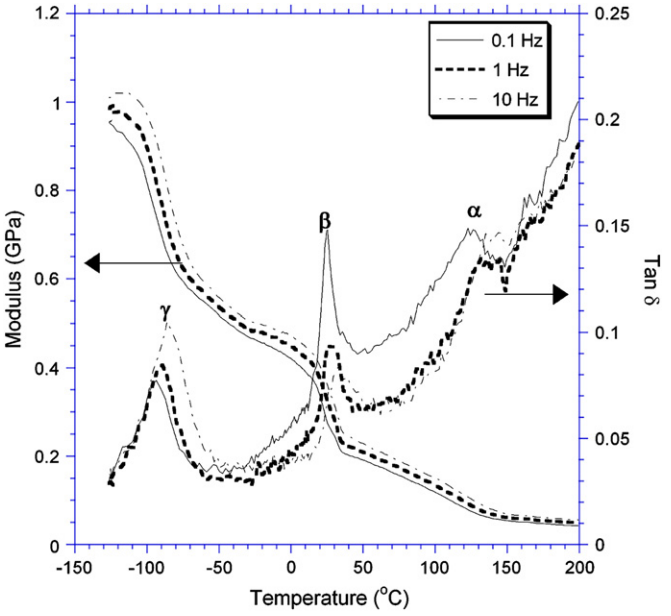

Fig. 3. Dynamic mechanical analysis of annealed PTFE.

relaxations of PTFE first reported by McCrum [13] are present in the DMA scans. The β peak is representative of a first order transition, while the α and γ peaks are second order transitions.

The effect of annealing to reduce the residual stresses is evident from the TMA data. In the radial (normal to extrusion) direction, there is little difference between the as-received and annealed samples. However, a large difference can be seen in the axial dimension (parallel to extrusion) change. This is expected since, during extrusion, the long polymer chains and crystallites align resulting in little dimension change with increasing temperature due to the inability of these aligned chains to stretch along the chain dimension. However, after annealing, the chains and crystallites become randomized in orientation. During a temperature scan, the chains have the ability to stretch and extend away from each other resulting in a dimension change comparable to that in the radial direction.

It can be seen from the DMA data in Fig. 3 that the phase transitions are dependent on the rate at which they were measured. It is not immediately obvious in Fig. 3 that the shift in the transition temperature per decade of strain rate is uniform. In order to determine whether the different rates are in fact linearly related, a correlation analysis is performed on the three data sets (at 0.1, 1, and 10 Hz) for both E and $\tan(\delta)$. The correlation coefficients are given as matrices for the three data sets:

$$\mathrm{Corr}(E) = \begin{bmatrix} 1.0000 & 0.9995 & 0.9977 \\ 0.9995 & 1.0000 & 0.9992 \\ 0.9977 & 0.9992 & 1.0000 \end{bmatrix},$$

$$\mathrm{Corr}(\tan\delta) = \begin{bmatrix} 1.0000 & 0.9682 & 0.9135 \\ 0.9682 & 1.0000 & 0.9787 \\ 0.9135 & 0.9787 & 1.0000 \end{bmatrix}.$$

It is immediately obvious that the modulus data are linearly dependent over the entire data set (>0.997) whereas the $\tan(\delta)$ is somewhat less correlated although still statistically significant (>0.9135). The lower correlation in the $\tan(\delta)$ data is likely due to the substantial relative noise.

The frequency at which the DMA temperature scans are conducted can be related to true strain rate using the following relationship:

$$\dot{\varepsilon} = \ln\left(\frac{t+d}{t}\right)\frac{f}{0.25} \tag{8}$$

where t is the specimen thickness, d is the maximum displacement amplitude during the cyclic load, and f is the frequency at which the temperature scan was performed. The maximum displacement is achieved in 0.25 cycles. In this case, 10 Hz frequency is equivalent to a strain rate of 0.05 s^{-1}. The location of the peak in $\tan(\delta)$ versus strain rate allows the temperature shift of the transitions to be calculated. The α, β, and γ peaks were found to shift by 3.8, 3.8, and 6.2 °C/decade strain rate, respectively. These shifts can then be used to calculate the approximate temperature at which the transitions would be expected to occur at higher rates and, therefore, to understand their effect on the measured mechanical behavior at high strain rates.

The fraction of both the as-received and annealed samples made up of the crystalline phase was quantified employing both density and DSC methods. In order to determine the mass fraction crystallinity from the DSC measurements, a heat of fusion (ΔH_f^0) for the 100% crystalline material was taken as 80 J g^{-1} and the following equation was used:

$$X_c = \frac{\Delta H_f(\text{sample})}{\Delta H_f^0}. \tag{9}$$

The mass fraction crystallinity is determined from density measurements using [4]:

$$X_c = \frac{(\rho - \rho_a)}{(\rho_c - \rho_a)}, \tag{10}$$

where ρ is the measured density of the sample, ρ_a is the extrapolated amorphous density (2040 kg/m^3) and ρ_c is the extrapolated crystalline density 2300 kg/m^3. The constants are taken directly from Rae and Dattelbaum [4], who in turn took them as the averages of the wide range of reported values from the literature as tabulated by Lehnert [38]. The measured densities, heats of fusion and calculated crystallinities are presented in Table 2 and Fig. 4. As a result of employing these literature values, these two methods do not provide consistent

Table 2
Densities, heat of fusion and calculated crystallinity for as-received and annealed PTFE compared to as-received PTFE 7C [4,11]

	Density (kg/m^3)	X_c	ΔH_f (J/g)	X_c
As-received PTFE	2177.1 ± 0.1	56 ± 1	31.0	39 ± 1
Annealed PTFE	2166.3 ± 0.1	52 ± 1	29.0	36 ± 1
As-received PTFE 7C	2168.9 ± 0.1	53 ± 1	30.3	38 ± 1

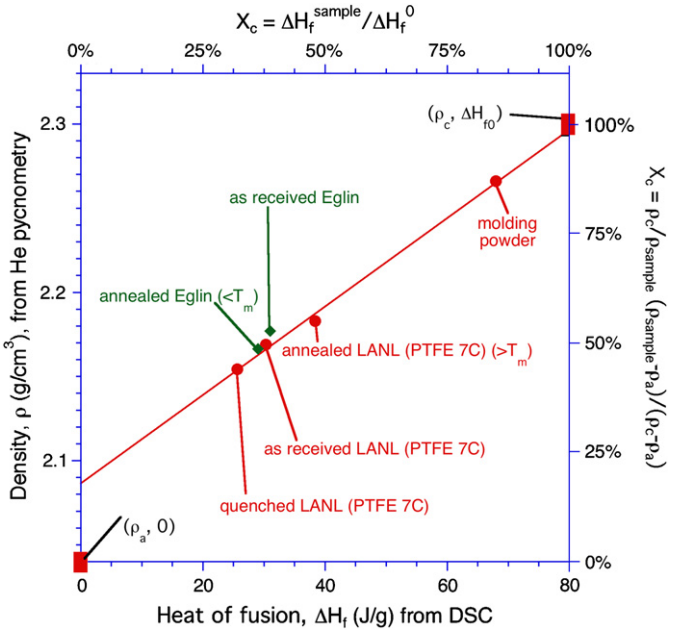

Fig. 4. Comparison of density, heat of fusion and crystallinity between as-received and annealed, below the melt, materials in this study and as-received and annealed, above the melt, PTFE from the LANL study [4].

solutions, which is why the linear fit through the data for PTFE 9B and PTFE 7C and literature values for 100% crystalline PTFE do not intercept the data point for 100% amorphous PTFE. One conclusion could be that the amorphous density should be taken to be $\rho_a = 2087\ \mathrm{kg/m^3}$. This would make the calculated results of Eqs. (9) and (10) much more consistent, but would be an arbitrary extrapolation and would make comparison of the current values to the literature more abstract. Lehnert [38] reported on the inconsistency between methods of calculating crystallinity in PTFE – showing equal or greater variation for other methods (IR, WAXS, NMR, etc.) – although all showed similar trends.

Both of these methods assume two distinct phases: unoriented amorphous and crystalline PTFE. They do not account for any porosity, which tends to be very low in PTFE, or the transition zones between the amorphous and crystalline regions. Moreover, PTFE cannot be manufactured as either purely amorphous or crystalline, so the values of ΔH_f^0, ρ_a, and ρ_c must all be extrapolated from experimental measurements. The DSC method captures only the mass fraction of purely thermodynamically crystalline PTFE and ΔH_f^0 is relatively invariant on the manufacturing process. The density method on the other hand is a much more empirical relationship and is sensitive to variations in the amorphous density associated with changes in free volume as determined by the manufacturing process and unoriented versus oriented amorphous structure. This latter point is particularly relevant in the current work where the as-received material exhibits strong anisotropy due to the extrusion process whereas the annealed material is much more isotropic.

It is worth noting that the range of crystallinities for the current study is relatively small compared to the study of Rae and Dattelbaum [4]. Moreover, the annealing process actually results in a small reduction in crystallinity in the current study rather than the significant increase shown in Fig. 4. In the current work the annealing process employed does not exceed the melt temperature of PTFE and is aimed at reducing the material's anisotropy. Increasing the crystallinity requires the additional mobility of the polymer chains achieved by a temperature excursion about the melt temperature. The slight reduction in crystalline fraction seen is likely due to disruption of the crystalline domains necessary for the reorientation of the amorphous domains.

3.2. Mechanical characterization

Mechanical characterization experiments were performed on the as-received and annealed PTFE at room temperature in the extrusion direction across a range of strain rates from 10^{-3} to $4 \times 10^5\ \mathrm{s^{-1}}$. The results are outlined in Figs. 5 and 6. In these figures, the curves represent averages of 3 to 5 experiments per strain rate, with approximately 4% variation between measured curves.

Specimen equilibrium in the high strain rate experiments was verified by comparing the one-wave stress, calculated from the transmitted pulse, and the two-wave stress, determined from the incident and reflected pulses, to determine if the two-wave stress oscillates around the one-wave stress [41,48]. It can be seen from Fig. 7(a) and (b) that this occurs in samples tested in both the SHPB and the MSHPB, for strain levels above 5 and 10%, respectively. In the SHPB samples, a constant strain rate is also observed. In the MSHPB samples, the strain rate increases slightly over the course of the

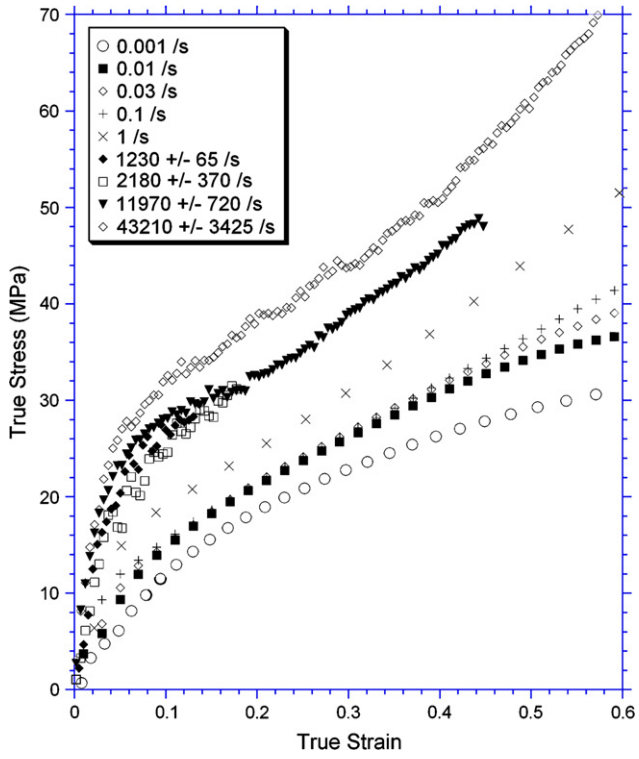

Fig. 5. As-received polytetrafluoroethylene tested in compression across a range of strain rates at room temperature.

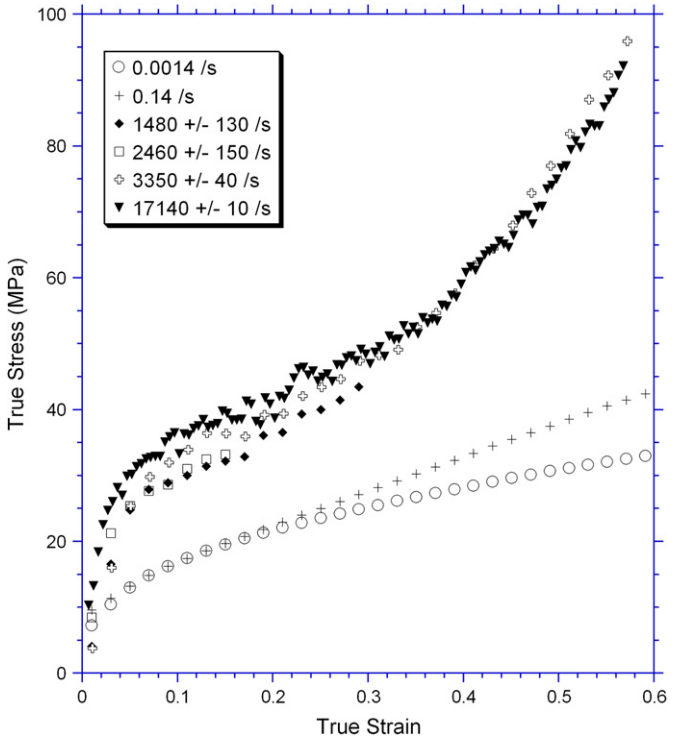

Fig. 6. Annealed polytetrafluoroethylene tested in compression across a range of strain rates at room temperature.

experiment but this can be corrected by careful choice of a wave-shaping (programming) material to alter the input pulse [41,48–51].

Comparison of the as-received and annealed PTFE is presented for three strain rates in Fig. 8(a–c). It can be seen that the annealed material has consistently higher strength than the as-received material at each rate. Generally, the strength of PTFE is thought to be proportional to the crystallinity percentage [4]. However, in the as-received versus annealed samples in this study, the opposite was found to be true, which agrees with studies performed on other semi-crystalline polymers [52]. It is hypothesized that the effect of alignment from extrusion plays a much greater role in the strength of the PTFE than the small difference in crystallinity between the as-received and annealed samples. In the as-received, extruded sample, the polymer chains are mainly aligned in the direction of the extrusion, which is also the direction of testing. This is confirmed by the TMA analysis where the behavior of the as-received material in the axial direction indicates much less axial expansion. When testing the as-received material in compression, the sample compresses in the direction of the chain alignment, while very little chain stretching in the radial direction occurs. However, the chains have a much more random orientation in the annealed sample as confirmed by the TMA data and, consequently, the expansions in the axial and radial directions are very similar (isotropic). In the annealed material, more regions of chains are therefore perpendicular to the loading direction, making it more difficult for the sample to expand radially and thus increasing the strength.

It is well known that polymers exhibit a rise in temperature associated with deformation, however, the authors put forward that the temperature increase during testing should be minimal and insufficient to drive the material through the phase IV to I transition. Rae and Dattelbaum [4] directly measured the temperature rise due to compressive deformation out to a true strain of 50% showing a temperature of less than 3 °C and concluding that the temperature excursion would not be sufficient for a phase transition. Additionally, Brown et al. [10] measured the yield stress of PTFE as a function of temperature at strain rates of 0.001 and 3200/s. While the observation of a change in slope of yield stress as a function of temperature associated with T_g is well documented to shift to higher temperatures with strain rate, the change in slope of yield stress as a function of temperature associated with the phase transition in PTFE occurs at constant temperature independent of strain rate. If the temperature rise was sufficient to push the materials through the phase transition, one would expect that the ambient temperature at which the phase

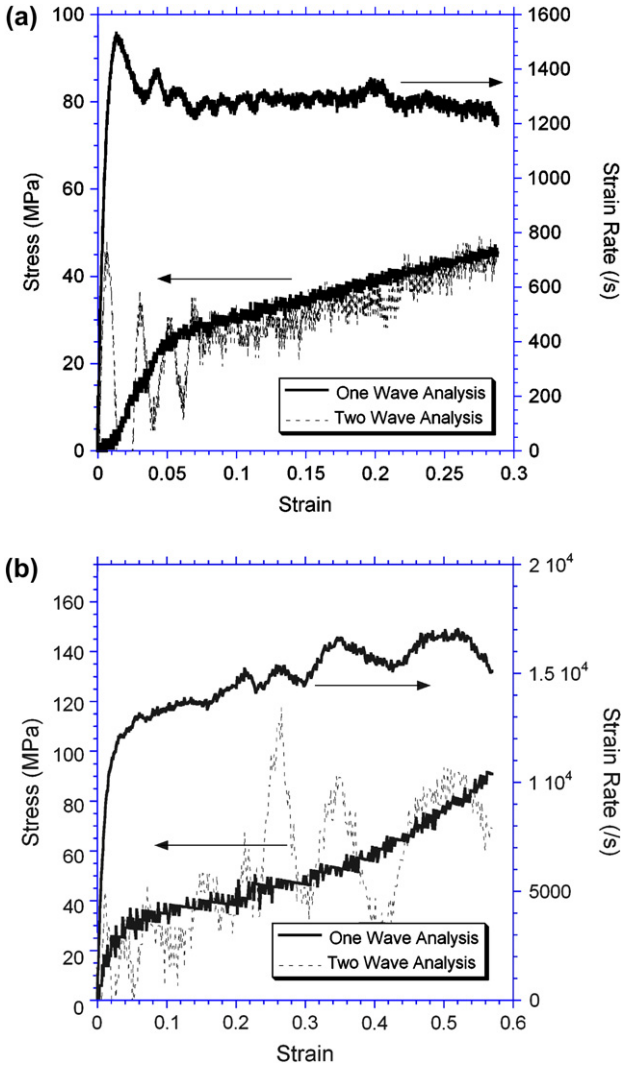

Fig. 7. One-wave versus two-wave stress analysis and strain rate versus strain for (a) split Hopkinson pressure bar and (b) miniaturized split Hopkinson pressure bar.

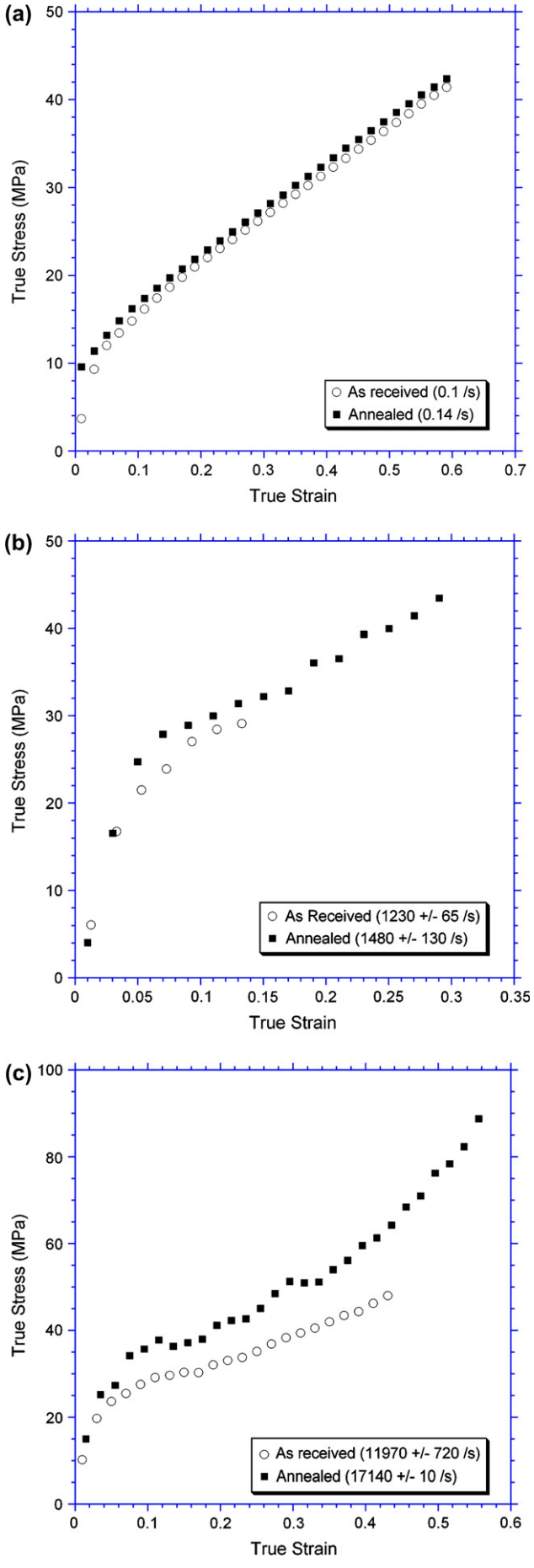

transition is observed would (a) be lower than the 30 °C temperature observed by DSC and (b) would shift to lower temperatures with increasing strain rate. Neither of these hold to be true. That said it is clear that there is a very distinct transition in phase II versus phase I. The temperature between tests prevents a clear observation on the phase IV response, other than saying it presents a smooth continuous transition between the phases.

From the measurements of radial and longitudinal strain, the Poisson's ratio of a number of specimens was calculated as a function of true strain, Fig. 9. Three curves for annealed samples tested at the same strain rate, ∼2300/s, are presented, in addition to a representative curve for the as-received samples at the same strain rate. At low strains the results are noisy due to the small size, and therefore relatively large error in the radial strains. However, in all cases the strains settle to an approximately constant value, 0.5 ± 0.1, at true strains of 0.1 and above, which corresponds to the sample having yielded and flowed. This is similar to observations by Rae and Dattelbaum [4] at quasi-static strain rates, where the data was taken from two strain gages mounted on the sample. The results indicate that volume is approximately conserved in the specimens during deformation. As well as giving useful insight for modeling purposes, these results support the use of volume conservation in the calculation of true specimen stress.

In order to compare the data acquired in this study on as-received and annealed, extruded PTFE 9B, with the data from other studies on PTFE [2−4], the strength at constant strain, 15%, was determined. It can be seen from Fig. 10 that, although the PTFE presented was prepared by different processing methods, the data follows the same general trend and exhibits a bilinear dependence of strength on $\log \dot{\varepsilon}$ at room temperature. However, there is some variability in the data presented, which, for the most part, is due to the different processing methods as well as types of PTFE − as-received and annealed PTFE 9b (this study), PTFE 7a and 7c (Rae and Dattelbaum [4]) and two unspecified forms (Walley and Field [1,3] and Gray et al. [2]). There is an outlying point in the Walley and Field [3] data at a strain rate of 0.016/s. An explanation for the scatter was not provided by the authors, but may be due to the different test apparatus used to acquire data at the wide range of strain rates presented in the paper.

A mapping, similar to that used by Siviour et al. [25,26], can be used to relate temperature to strain rate for PTFE data from this study and from the literature. The aim of this mapping is to provide an understanding of how the lower order transitions (in this case β and γ) affect the strength of a polymer at high strain rates. In particular, it was motivated by a requirement to understand the bilinear dependence of the strength of many polymers on $\log(\dot{\varepsilon})$. Firstly, it is noted that increasing the temperature at which an experiment is performed is linearly equivalent to decreasing $\log(\dot{\varepsilon})$. Therefore, a series of experiments performed at a range of temperatures and strain rates can be mapped to a single 'master' curve of

Fig. 8. Comparison between as-received and annealed PTFE at (a) quasi-static, (b) intermediate and (c) high strain rates at room temperature.

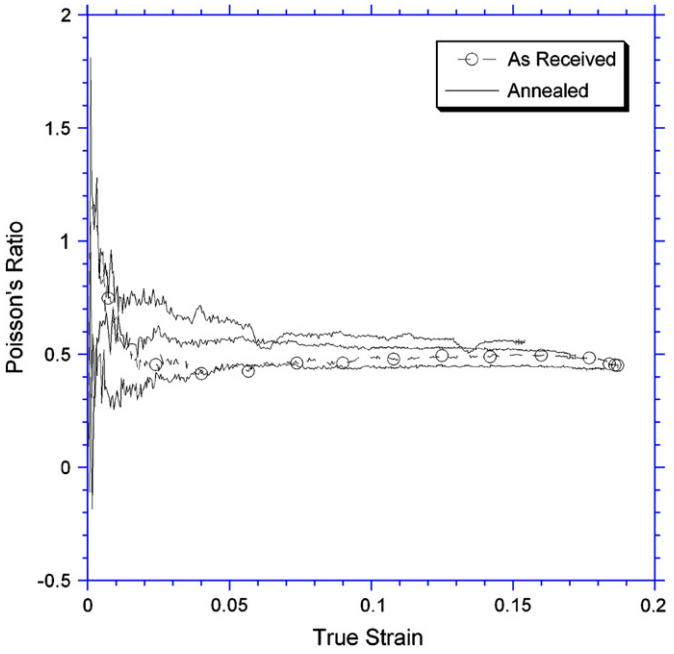

Fig. 9. Poisson's ratio as a function of true strain for as-received and annealed PTFE determined from in situ laser diameter measurement and high speed photographic record.

strength against equivalent temperature (T_{map}) at a single strain rate (ε_{map}). This is a pragmatic, empirically based linearization and extension to large strains of the well-known WLF formula [53]. The master curve produced by this mapping can then be compared directly to DMA data from the same material. In addition the DMA data also allow evaluation of the frequency (or strain rate) dependence of the temperatures at which the lower order transitions occur. *Careful* extrapolation of this dependence to high strain rates and comparison to the 'master' curve allows the different gradients of the master curve to be related to the lower order transitions. Comparison back to the curve of strength against $\log(\dot{\varepsilon})$ further allows the dependence of this strength to be understood in terms of lower order transitions. Effectively, we are seeing the strain rate at which lower order transition temperatures shift to room temperature.

In order to apply the mapping, a suitable strain rate $\dot{\varepsilon}_{map}$ is first chosen. This is most conveniently one of the strain rates that was used in the experimental program, and in this case two rates were used: 0.1 s^{-1} and 3200 s^{-1}. The value T_{map}, is defined as

$$T_{map} = T_{exp} + A\left(\log\left(\dot{\varepsilon}_{map}\right) - \log\left(\dot{\varepsilon}_{exp}\right)\right) \tag{11}$$

where the subscript exp indicates the experimental values of strain rate and temperature. A is a constant fit from the experimental data, giving a value of $A = 8$. Mapping the experimental data presented in Fig. 10 to 0.1 s^{-1} and 3200 s^{-1} results in the curves presented in Fig. 11. This mapping is important for three reasons:

(1) It allows more accurate comparison of experimental studies performed at slightly different strain rates and temperatures. In particular, small changes in temperature have a large effect on polymer strength, and data which look disparate in Fig. 10 are brought closer together by taking this into account.
(2) By relating the strain rate dependence of the material to its temperature dependence, it is confirmed that the bilinear relationship between strength and strain rate is a material property, and is not the result of inertia or equilibrium effects in the high strain rate experiments.

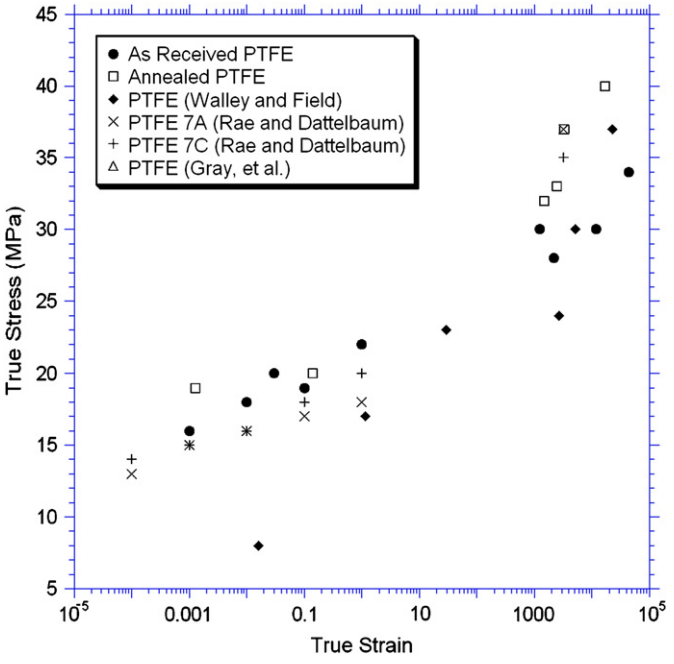

Fig. 10. Comparison of PTFE strength at room temperature and 15% strain with data from Walley and Field [1], Rae and Dattelbaum [4], and Gray et al. [2].

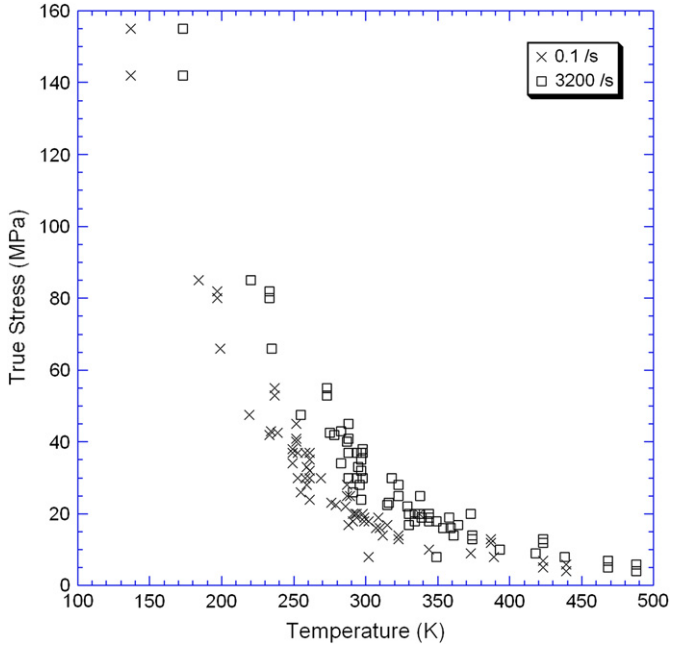

Fig. 11. PTFE strength data from this study, Walley et al. [1], Rae and Dattelbaum [4], and Gray et al. [2] mapped to 0.1 s^{-1} and 3200 s^{-1}.

(3) Curves such as this allow us to relate the large-strain behavior to the effect of different material transitions. In this case, it is seen that the bilinear strain rate response is due to the γ transition in PTFE.

However, care must be taken when interpreting these data. Firstly, it is noted that the data in Figs. 10 and 11 are similar to yield strengths, whereas the DMA data are small strain moduli. This means that the typical WLF constants for a material will not necessarily be the same as the constant in Eq. (11). Further, the polymer transitions have different dependences on frequency, typically they are spaced closer together at higher frequencies.[2] Overall, therefore the gradients observed in Fig. 11 are not directly comparable to those in the DMA data – however, the *position* of the transitions on the temperature axis does not depend on whether modulus or yield strength is used. Thus, the extrapolation of the transition temperatures to high strain rate should give the correct positions (see also Refs. [25–27]), as would an ultra-high frequency DMA experiment. Finally, it should be noted that some phase changes (e.g. melting) are not frequency dependent and occur at the temperature at high strain rates as they do in the DMA.

3.3. Application of the Zerilli–Armstrong model

The Zerilli–Armstrong model for polymers was implemented and compared to the static and dynamic stress–strain data using a Matlab-based code. The code iteratively solves Eq. (1), using a built-in explicit Runge–Kutta solver (*ode45*), embedded within a model-based maximum a posteriori estimator to determine the model coefficients. The value of plastic strain rate at each iteration is found by equating the sum of the viscous stresses and the plastic stress and solving for plastic strain rate which is found through a root-finding routine (*fzero*). The total strain rate is assumed to be constant. The behavior of the model at low strain rates ($<10^{-3}\ s^{-1}$) was problematic in the analysis. The available solvers do not have explicit control of the time stepping function and tended to fail to converge due to insufficient sampling. The problem was ultimately diagnosed as numerical instability associated with the very low flow mobilities. Although this problem only occurs at low strain rates and therefore is still useful for the majority of this data, it is recognized as a limitation of our approach and is being addressed.

The Zerilli–Armstrong model, using the constants presented in Ref. [36]. Tables 1 and 2 are compared to experimental data from this study, shown in Fig. 12. The percent difference between the experiment and the model,

$$\%\text{difference} = |\text{experimental} - \text{model}|/\text{experimental} \quad (12)$$

varies from 10–30% depending on the strain rate, after the initial elastic region, which compares with the agreement between the model and the Walley and Field [1] data, as discussed by Zerilli and Armstrong [34]. At small strains, the model overpredicts the stress due to the lack of a rate dependence in the initial modulus. Additionally, at high strains the model overpredicts the amount of strain hardening seen experimentally. This overprediction could be improved by calibrating the model to the experimental data in this study,

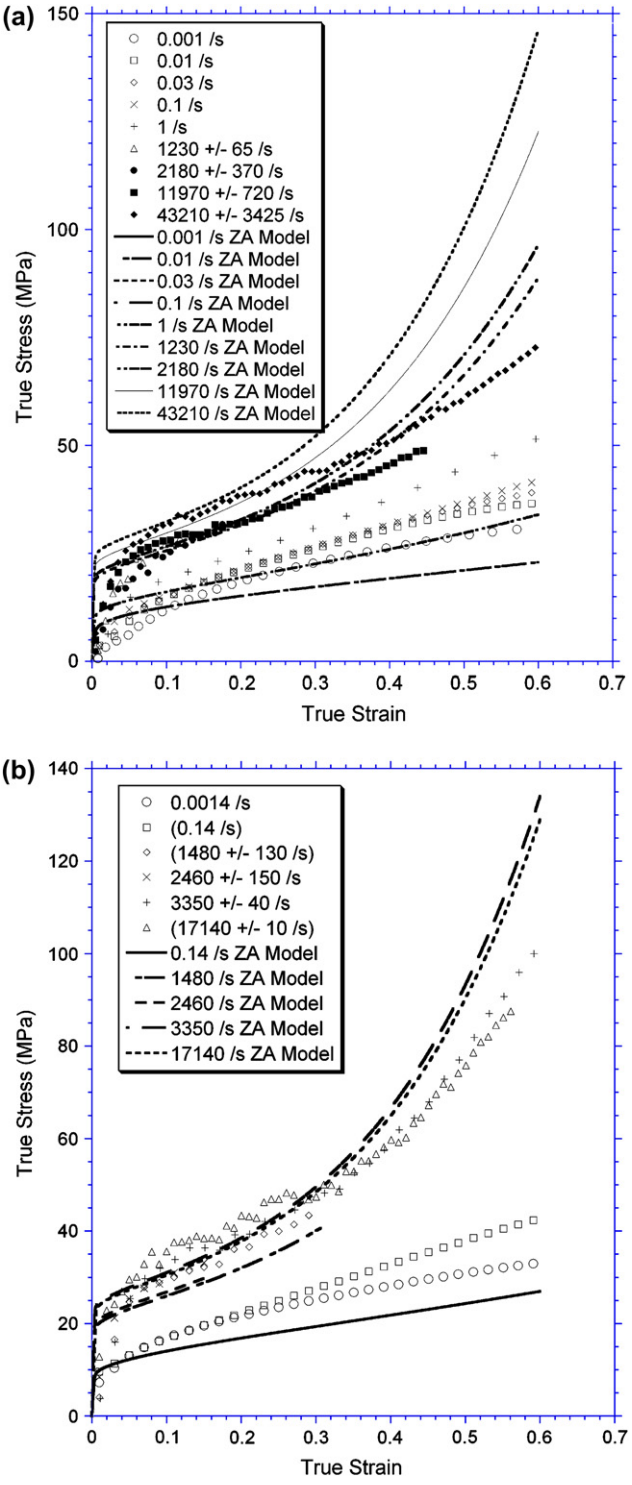

Fig. 12. Comparison of Zerilli–Armstrong model to (a) as-received and (b) annealed PTFE experimental data using published parameters [36].

[2] In fact, if the experimental data showed less scatter, it may be necessary to use a larger number of parameters to take this into account.

as the comparison to data from Walley and Field shows better agreement at large strains [34].

4. Conclusions

The properties of extruded, as-received, and annealed Dupont 9B polytetrafluoroethylene (PTFE) were investigated at strain rates from 10^{-3} to $10^{5}\ s^{-1}$. The annealed PTFE had lower crystallinity and yet showed anomalously higher strength than the as-received PTFE, which was attributed to the orientation of the polymer chains during the extrusion process. The data measured in this study was compared to that presented in the literature, and the bilinear stress–strain rate relationship was confirmed using time–temperature superposition. Whilst the different transitions in PTFE cause more spread in these data than in previous studies on different polymers, the results allow the dependence of the bilinear relationship attributed to the γ transition. Finally, the experimental data was analyzed using the Zerilli–Armstrong model for polymers with reasonable agreement to experimental values.

Acknowledgements

The authors would like to thank AFRL/MNME and AFRL/MNMF for sponsoring this research. Dr. Eric N. Brown acknowledges the Joint DoD/DOE Munitions program. The thermal analysis (DSC and TMA) presented in this work was conducted by Mr. Pete Stevens, Properties Team, Development Section, Energetic Materials Branch. The authors would like to thank Dr. David Williamson, Cavendish Laboratory, for conducting DMTA analysis. Dr. Frank Zerilli, NSWC – Indian Head, provided invaluable advice and guidance as to the implementation of the Zerilli–Armstrong model for polymers. Finally, we would like to thank Dr. W.G. Proud, Dr. S.M. Walley and Professor J.E. Field for useful advice and support.

Opinions, interpretations, conclusions, and recommendations are those of the authors and not necessarily endorsed by the United States Air Force.

References

[1] Walley SM, Field JE, Pope RH, Safford NA. The rapid deformation behaviour of various polymers. Journal de Physique III France 1991; 1:1889–925.
[2] Gray III GT, Cady CM, Blumenthal WR. Influence of temperature and strain rate on the constitutive behavior of Teflon and Nylon. In: Plasticity '99: the seventh international symposium on plasticity and its current applications; 1999.
[3] Walley SM, Field JE. Strain rate sensitivity of polymers in compression from low to high rates. DYMAT Journal 1994;1(3):211–27.
[4] Rae PJ, Dattelbaum DM. The properties of poly(tetrafluoroethylene) (PTFE) in compression. Polymer 2004;45(22):7615–25.
[5] Rae PJ, Brown EN. The properties of poly(tetrafluoroethylene) (PTFE) in tension. Polymer 2005;46(19):8128–40.
[6] Rae PJ, Brown EN, Clements BE, Dattelbaum DM. Pressure-induced phase change in poly(tetrafluoroethylene) at modest impact velocities. Journal of Applied Physics 2005;98:1–8.
[7] Brown EN, Dattelbaum DM. The role of crystalline phase on fracture and microstructure evolution of polytetrafluoroethylene (PTFE). Polymer 2005;46:3056–68.
[8] Brown EN, Trujillo CP, Gray III GT, Rae PJ, Bourne NK. Soft-recovery of polytetrafluoroethylene shocked through crystallizing phase II–III transition. Journal of Applied Physics 2007;101(2):024916.
[9] Brown EN, Clausen B, Brown DW. In situ measurement of crystalline lattice strains in phase IV polytetrafluoroethylene. Journal of Neutron Research, in press.
[10] Brown EN, Rae PJ, Gray III GT. The influence of temperature and strain rate on the tensile and compressive constitutive properties of four fluoropolymers. Journal de Physique IV France 2006;134:935–40.
[11] Brown EN, Rae PJ, Orler BE, Gray GT, Dattelbaum DM. The effect of crystallinity on the fracture of polytetrafluoroethylene (PTFE). Materials Science and Engineering C 2006;8:1338–43.
[12] Starkweather HW. A comparison of the rheological properties of polytetrafluoroethylene below its melting point with certain low-molecular smectic states. Journal of Polymer Science 1979;17:73–9.
[13] McCrum NG, Read BE, Williams G. Anelastic and dielectric effects in polymeric solids. New York: Wiley; 1959.
[14] Sauer JA, Pae KD. The flow of solid polymers under high pressure. Colloid and Polymer Science 1974;252:680–95.
[15] Chou SC, Robertson KD, Rainey JH. The effect of strain rate and heat developed during deformation on the stress–strain curve of plastics. Experimental Mechanics 1973;13:422–32.
[16] Briscoe BJ, Hutchings IM. Impact yielding of high density polyethylene. Polymer 1976;17:1099–102.
[17] Kukureka SN, Hutchings IM. Measurement of the mechanical properties of polymers at high strain rates by Taylor impact. In: Blazynski TZ, editor. Proceedings of the seventh international conference on high energy rate fabrication. Leeds: University of Leeds; 1981. p. 29–38.
[18] Briscoe BJ, Nosker RW. The influence of interfacial friction on the deformation of high density polyethylene in a split Hopkinson pressure bar. Wear 1984;95:241–62.
[19] Briscoe BJ, Nosker RW. The flow stress of high density polyethylene at high rates of strain. Polymer Communication 1985;26:307–8.
[20] Brown EN, Willms RB, Gray III GT, Rae PJ, Cady CM, Vecchio KS, et al. Influence of molecular conformation on the constitutive response of polyethylene: a comparison of HDPE, UHMWPE, and PEX. Experimental Mechanics 2007;47(3):381–93.
[21] Bauwens-Crowet C. The compression yield behaviour of PMMA over a wide range of temperature and strain rates. Journal of Materials Science 1973;8:968–79.
[22] Bauwens JC. Relation between the compression yield stress and the mechanical loss peak of bisphenol-A-polycarbonate in the β transition range. Journal of Materials Science 1972;7:577–84.
[23] Bauwens-Crowet C, Bauwens JC, Homès G. The temperature dependence of yield of polycarbonate in uniaxial compression and tensile tests. Journal of Materials Science 1972;7:176–83.
[24] Rietsch F, Bouette B. The compression yield behaviour of PC over a wide range of strain rates and temperatures. European Polymer Journal 1990;26:1071–5.
[25] Siviour CR, Walley SM, Proud WG, Field JE. Mechanical behaviour of polymers at high rates of strain. Journal de Physique IV 2006;134: 949–55.
[26] Siviour CR, Walley SM, Proud WG, Field JE. The high strain rate compressive behavior of polycarbonate and polyvinylidene fluoride. Polymer 2005;46:12546–55.
[27] Mulliken AD, Boyce MC. Mechanics of the rate-dependent elastic–plastic deformation of glassy polymers from low to high strain rates. International Journal of Solids and Structures 2006;43(5):1331–56.
[28] Khan A, Zhang H. Finite deformation of a polymer: experiments and modeling. International Journal of Plasticity 2001;17(9):1167–88.
[29] Kletschkowski T, Schomburg U, Bertram A. Endochronic viscoplastic material models for filled PTFE. Mechanics of Materials 2002;34(12):795–808.
[30] Bergstrom JS, Hilbert JLB. A constitutive model for predicting the large deformation thermomechanical behavior of fluoropolymers. Mechanics of Materials 2005;37(8):899–913.

[31] Zerilli FJ, Armstrong RW. Application of Eyring's thermal activation theory to constitutive equations for polymers. In: Shock compression of condensed matter – 1999. Snowbird, UT: American Institute of Physics; 1999.
[32] Zerilli FJ, Armstrong RW. Thermal activation based constitutive equations for polymers. Journal de Physique IV France 2000;10(9):3–8.
[33] Zerilli FJ, Armstrong RW. A constitutive equation for dynamic deformation behavior of polymers. Naval Surface Warfare Center – Indian Head; 2000.
[34] Zerilli FJ, Armstrong RW. Thermal activation constitutive model for polymers applied to polytetrafluoroethylene. In: Shock compression of condensed matter – 2001. Atlanta, GA: American Institute of Physics; 2002.
[35] Zerilli FJ. Dislocation mechanics-based constitutive equations. Metallurgical and Materials Transactions A 2004;35A:2547–55.
[36] Zerilli FJ, Armstrong RW. A constitutive equation for the dynamic deformation behavior of polymers. Journal of Materials Science 2007.
[37] Teflon PTFE 9B, fluoropolymer resin. Dupont Product Information, 1999.
[38] Lehnert RJ, Hendra PJ, Everall N, Clayden NJ. Comparative quantitative study on the crystallinity of poly(tetrafluoroethylene) including Raman, infra-red and F-19 nuclear magnetic resonance spectroscopy. Polymer 1997;38(7):1521–35.
[39] Pucciariello R, Villani V. Melting and crystallization behavior of poly(tetrafluoroethylene) by temperature modulated calorimetry. Polymer 2004;45(6):2031–9.
[40] Androsch R, Wunderlich B, Radusch HJ. Analysis of reversible melting in polytetrafluoroethylene. Journal of Thermal Analysis and Calorimetry 2005;79(3):615–22.
[41] Gray III GT. In: Kuhn H, Medlin D, editors. Classic split-Hopkinson pressure bar testing, in ASM handbook. Mechanical testing and evaluation, vol. 8. ASM International: Materials Park; 2002. p. 462–76.
[42] Tasker DG, Dick RD, Wilson WH. Mechanical properties of explosives under high deformation loading conditions. In: Shock compression of condensed matter – 1997. American Institute of Physics; 1998.
[43] Gorham DA. Measurement of stress–strain properties of strong metals at very high rates of strain. Institute of Physics Conference Series 1979; 47:16–24.
[44] Gorham DA, Pope PH, Field JE. An improved method for compressive stress strain measurement at very high strain rates. Proceedings of the Royal Society of London 1992;438:153–70.
[45] Mentha SN, Pope PH, Field JE. Progress in metal testing with a 3 mm pressure bar. Institute of Physics Conference Series 1984;70:175–6.
[46] Jia D, Ramesh KT. A rigorous assessment of the benefits of miniaturization in the Kolsky bar system. Experimental Mechanics 2004;44: 445–54.
[47] Ramesh KT, Narasimhan S. Finite deformations and the dynamic measurement of radial strains in compression Kolsky bar experiments. International Journal of Solids and Structures 1996;33(25):3723–38.
[48] Gray III GT, Blumenthal WR. Split-Hopkinson pressure bar testing of soft materials. In: Kuhn H, Medlin D, editors. Mechanical testing and evaluation. ASM handbook, vol. 8. Materials Park: ASM International; 2000. p. 488–96.
[49] Frantz CE, Follansbee PS, Wright WT. Experimental techniques with the split Hopkinson pressure bar. In: The eighth international conference on high energy rate fabrication; 1984.
[50] Frew DJ, Forrestal MJ, Chen W. A split hopkinson pressure bar technique to determine compressive stress–strain data for rock materials. Experimental Mechanics 2001;41(1):40–6.
[51] Frew DJ, Forrestal M, Chen W. Pulse shaping techniques for testing elastic–plastic materials with a split Hopkinson pressure bar. Experimental Mechanics 2005;45:186–95.
[52] Lee CS, Caddell RM, Yeh GSY. Cold extrusion and cold drawing of polymeric rod: the influence on subsequent tensile and compressive mechanical properties. Materials Science and Engineering 1972;10: 241–8.
[53] Williams ML, Landel RF, Ferry JD. The temperature dependence of relaxation mechanisms in amorphous polymers and other glass-forming liquids. Journal of American Chemical Society 1955;77:3701–7.